Journal of Magnetic Resonance 246 (2014) 9–17

Contents lists available at ScienceDirect

Journal of Magnetic Resonance

journal homepage: www.elsevier.com/locate/jmr

Spectral editing through laser-flash excitation in two-dimensional photo-CIDNP MAS NMR experiments

Karthick Babu Sai Sankar Gupta [a], Eugenio Daviso [a,b], Gunnar Jeschke [c], A. Alia [a,d], Matthias Ernst [c], Jörg Matysik [a,d,*]

[a] Leiden Institute of Chemistry, Leiden University, P.O. Box 9502, 2300 RA Leiden, The Netherlands
[b] Francis Bitter Magnet Laboratory, Albany Street 150, NW14, Cambridge, MA 02139, USA
[c] ETH Zürich, Physical Chemistry, Wolfgang-Pauli-Strasse 10, 8093 Zürich, Switzerland
[d] Institut für Analytische Chemie, Universität Leipzig, Linnéstr. 3, 04103 Leipzig, Germany

ARTICLE INFO

Article history:
Received 29 April 2014
Revised 8 June 2014
Available online 27 June 2014

Keywords:
Photo-CIDNP
MAS NMR
Spectral editing
Hyperfine interaction
laser excitation
DARR

ABSTRACT

In solid-state photochemically induced dynamic nuclear polarization (photo-CIDNP) MAS NMR experiments, strong signal enhancement is observed from molecules forming a spin-correlated radical pair in a rigid matrix. Two-dimensional ^{13}C–^{13}C dipolar-assisted rotational resonance (DARR) photo-CIDNP MAS NMR experiments have been applied to obtain exact chemical shift assignments from those cofactors. Under continuous illumination, the signals are enhanced via three-spin mixing (TSM) and differential decay (DD) and their intensity corresponds to the electron spin density in p_z orbitals. In multiple-^{13}C labelled samples, spin diffusion leads to propagation of signal enhancement to all ^{13}C spins. Under steady-state conditions, direct signal assignment is possible due to the uniform signal intensity. The original intensities, however, are inaccessible and the information of the local electron spin density is lost. Upon laser-flash illumination, the signal is enhanced via the classical radical pair mechanism (RPM). The obtained intensities are related to isotropic hyperfine interactions a_{iso} and both enhanced absorptive and emissive lines can be observed due to differences in the sign of the local isotropic hyperfine interaction. Exploiting the mechanism of the polarization, selectivity can be increased by the novel time-resolved two-dimensional dipolar-assisted rotational resonance (DARR) MAS NMR experiment which simplifies the signal assignment compared to complex spectra of the same RCs obtained by continuous illumination. Here we present two-dimensional time-resolved photo-CIDNP MAS NMR experiments providing both directly: signal assignment and spectral editing by sign and strength of a_{iso}. Hence, this experiment provides a direct key to the electronic structure of the correlated radical pair.

1. Introduction

The discovery of the solid-state photo-CIDNP (photochemically induced dynamic nuclear polarization) effect (for reviews: [1,2]) by Zysmilich and McDermott in 1994 in frozen and quinone-blocked bacterial reaction centers (RCs) of *Rhodobacter* (*R.*) *sphaeroides* R26 by ^{15}N magic-angle spinning (MAS) NMR under continuous illumination with white light offered a new experimental access to electron–nuclear processes during charge separation [3]. By induction of a non-Boltzmann nuclear spin polarization, enhancement of signals of a factor of more than 80,000 has been observed from the nuclei of the cofactors forming the light-induced radical pair [4–7]. In recent years, the solid-state photo-CIDNP effect has also been observed in several photosynthetic RCs, as those obtained from the purple bacteria *R. sphaeroides* wildtype (WT) [4] and R26 [3,5,7], *Rhodopseudomonas acidophila* [8], the green sulfur bacterium *Chlorobium tepidum* [9], the heliobacterium *Heliobacillus mobilis* [6] as well as of the photosystems I and II of plants [10–12] and algae [13]. The occurrence of the solid-state photo-CIDNP effect appears to be an intrinsic property of natural photosynthetic RCs [14]. Recent observation of the effect in a blue-light photoreceptor [15] demonstrates that the effect is not limited to natural photosynthesis.

In RCs of *R. sphaeroides*, light absorption induces charge separation within 3 ps from the primary donor (P) formed by 2 bacteriochlorophyll *a* (BChl) to the primary acceptor, a bacteriopheophytin (Φ_A) (for review, see [16]) (Fig. 1A and B). The radical pair is initially in a singlet state (Fig. 2). From this singlet state,

* Corresponding author at: Institut für Analytische Chemie, Universität Leipzig, Linnéstr. 3, 04103 Leipzig, Germany. Fax: +49 341 9736115.
E-mail address: joerg.matysik@uni-leipzig.de (J. Matysik).

http://dx.doi.org/10.1016/j.jmr.2014.06.007
1090-7807/

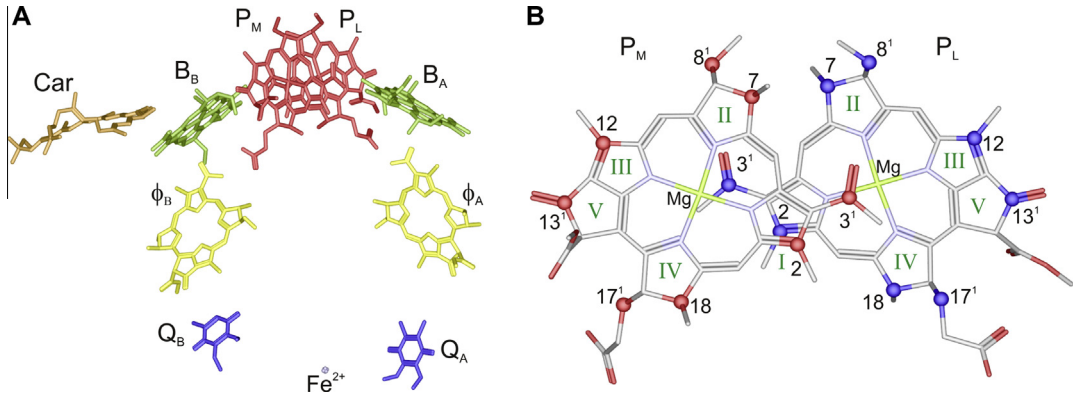

Fig. 1. (A) Arrangement of cofactors in reaction centers (RCs) of *Rhodobacter (R.) sphaeroides* wildtype (WT). The primary electron donor, the special pair, is formed by the two bacteriochlorophyll *a* (BChl) molecules P_M and P_L. B_A and B_B are accessory BChl cofactors, Φ_A and Φ_B are bacteriopheophytin (BPhe) cofactors. On the acceptor side, two ubiquinone-10 cofactors Q_A and Q_B are located with a non-heme iron in between. The symmetry of the cofactor arrangement is broken by a carotenoid (Car) cofactor. The light-induced electron transfer occurs selectively via branch A. (B) The spatial arrangement of the two cofactors P_L (right, isotope labels in blue) and P_M (left, isotope labels in red) forming the special pair. The pyrrole rings are numbered with green Roman numbers. Both pyrrole rings I are overlapping. The isotope labelling pattern has been obtained by feeding with 3-$^{13}C_1$-δ-aminolevulinic acid (3-ALA, see Fig. 4). The long side chains are omitted to provide a better view on the arrangement of the active elements in the charge separation process. [pdb entry 1M3X, (Camara-Artigas et al., 2002b) the figure has been made with Accelrys Discovery Studio]. (For interpretation of the references to color in this figure legend, the reader is referred to the web version of this article.)

photochemically induced dynamic electron polarization (photo-CIDEP) is observed as strongly enhanced absorptive and emissive signals in the EPR spectrum [17,18]. During the lifetime of the radical pair, the electron–spin system oscillates between the singlet state (S) [$^1(P^+\Phi_A^{\cdot-})$] of the radical pair and the triplet state (T_0) [$^3(P^+\Phi_A^-)$] with a frequency that depends on both the hyperfine interaction and the difference of the electron Zeeman interaction.

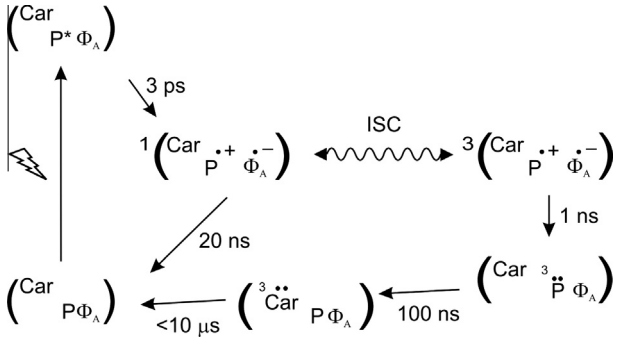

Fig. 2. Kinetics and spin dynamics of electron transport in quinone-depleted RCs of *R. sphaeroides* wild type (WT). After absorption of a photon the photochemically excited state of the primary donor P^* is formed and an electron is transferred to the primary acceptor Φ_A, a bacteriopheophytin cofactor. Initially, the radical pair is in its singlet state $^1(P^+\Phi_A^{\cdot-})$. It evolves into a triplet state $^3(P^+\Phi_A^{\cdot-})$ due to the electronic interactions and hyperfine coupling with nearby nuclei, a process which is known as intersystem crossing (ISC). The radical-pair mechanism (RPM) leads to sorting of nuclear spins via the isotropic hyperfine coupling, but without a net increase of the population difference of the spin up and the spin down nuclear states. In the TSM, hyperfine coupling, nuclear and electronic Zeeman interactions, and anisotropic interactions involving electrons and nuclei lead to symmetry breaking and net nuclear polarization that can be observed both in laser excitation experiments and under steady-state conditions. The lifetime for recombination from the singlet state to the ground state is 20 ns, while charge recombination from the $^3(P^+\Phi_A^{\cdot-})$ radical pair state forms a donor triplet state ^3P with a time constant of 1 ns. With continuous illumination the difference in recombination rates from the singlet and triplet states to the neutral ground state also break the symmetry when they match the inverse of the pseudosecular component of the hyperfine interaction, a process that is known as the DD mechanism. For the WT, the ^3P is rapidly converted (100 ns) in a carotenoid triplet (^{3}Car) and followed by a much slower decay from the carotenoid triplet state to the ground state. Time-resolved experiments have shown that a large fraction of the excited state decays via ^{3}Car, in competition with back conversion to the $^3(P^+\Phi_A^-)$ that decays rapidly with 20 ns to establish the steady state. Before reaching this steady state, however, transient effects from RPM, TSM and DD can be observed with time-resolved photo-CIDNP, on a timescale of 10 µs and different mechanisms can be resolved by adjusting the time between the photo-CIDNP excitation and the NMR detection scheme.

The coherent interconversion from singlet to triplet radical pairs and back gives rise to spin sorting within the scheme of the well-known radical pair mechanism (RPM) (Fig. 2) [19,20]. Under continuous illumination (CI), the RPM does not induce signal enhancement because the reaction products of both decay branches are have opposite sign and cancel exactly.

In solid-state photo-CIDNP MAS NMR experiments under CI, two additional solid-state mechanisms run in parallel to induce *net* nuclear polarization which remains under steady-state conditions (Fig. 2) [1,2]: (i) Electron–electron–nuclear three-spin mixing (TSM) breaks the balance by coherent evolution of the correlated radical pair state in interaction with the nuclear spins and the applied magnetic field, depending on the signs of the electron–electron and of the anisotropic electron–nuclear interactions [21,22]. (ii) In the electron–nuclear differential decay (DD) mechanism [23], the symmetry is broken by different lifetimes of the S [$^1(P^+\Phi_A^{\cdot-})$] and of the T_0 [$^3(P^+\Phi_A^{\cdot-})$] states. The dependence of secular part of the hyperfine coupling A is the only single matching of interactions $2|\omega_I| = |A|$ is required and the difference of singlet and triplet radical pair lifetimes must be of the order of the inverse hyperfine coupling [1]. A more detailed analysis shows [24] that ^{13}C the hyperfine coupling anisotropy ΔA required for these solid-state mechanisms scales with the local electron spin density in the p_Z orbitals of the π system of the radical cation state. Photo-CIDNP intensities in this regime are roughly proportional to ΔA^2 [1].

In time-resolved experiments on RCs of *R. sphaeroides* WT, transient nuclear polarization has been observed long as 10 µs [25]. The decay from the singlet state to the ground state is 20 ns, much faster than the pathway via the donor triplet state ^3P, which is rate limited by the decay from the carotenoid triplet state to the ground state, i.e., 10 µs (Fig. 1). Thus, transient nuclear polarization can be observed, originating from the nuclear polarization associated with rapid decay of the $^1(P^+\Phi_A^{\cdot-})$ state while the polarization associated with the decay of the ^3P channel is hidden by the paramagnetic triplet state of the carotenoid (^{3}Car) during its lifetime. As a result, the nuclear polarization of the triplet decay channel cannot be detected on the nearby nuclei in experiments with a short delay <10 µs between optical excitation and NMR detection (Fig. 2) [2,25]. Hence, transiently, using time-resolved experiments, RPM nuclear polarization can be observed under solid-state conditions since the triplet decay rate differs from the singlet one [25]. The sign of the transient light-induced signals follows Kaptein's sign

rules [26]. According to those rules, in the RPM the sign depends on the spin state of the precursor, the decay path of the radical pair, and the signs of Δg of the radical pair and of the hyperfine (hf) constant. If, as in our case, the first three parameters are given by the system, the sign and signal intensity are directly correlated to the hf constant a_{iso}.

Hence, time-resolved photo-CIDNP MAS NMR nuclear intensities allows to map isotropic electron spin densities and corresponding hf interaction constants (a_{iso}) on the donor with atomic selectivity [27]. Interpretation of the one-dimensional envelope of transient nuclear polarization requires chemical shift assignments, which have been obtained in separate continuous-illumination experiments. Here we show that two-dimensional nanosecond laser-flash photo-CIDNP MAS NMR experiments measure both, chemical shifts, that are unambiguously assigned, and local electron spin densities in a single experiment.

2. Methodology

2.1. Dipolar assisted rotational resonance (DARR) spectroscopy

To explore connectivities between carbons, ^{13}C–^{13}C homonuclear shift-correlation experiments are available. In solid state MAS NMR, several pulse sequences have been developed for homonuclear correlations, such as DRAMA [28], RFDR [29,30], C7 [31], PDSD [32,33] and DARR [34]. More on dipolar recoupling could found on these review articles [35,36]. In the DARR (Dipolar assisted rotational resonance) experiment, nuclear polarization transfer is driven by a spin-diffusion-type mechanism while the heteronuclear (^{1}H–^{13}C) dipolar couplings are re-established by continuous ^{1}H rf irradiation on a rotary resonance condition [37]. The pulse sequence for the DARR experiment is shown in Fig. 3A. In the preparation period, a standard cross polarization (CP) step

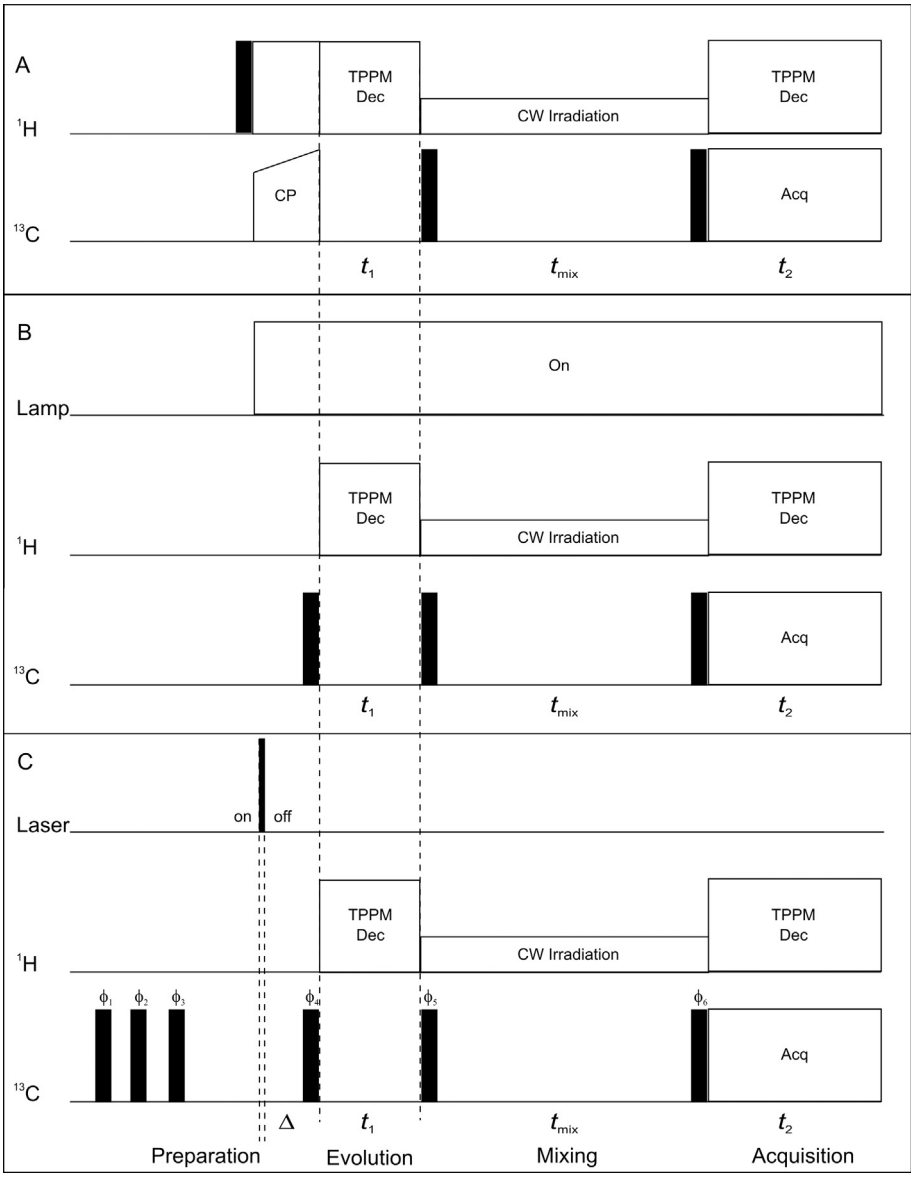

Fig. 3. Two-dimensional ^{13}C–^{13}C CP DARR MAS NMR pulse program. Solid bars indicate the $\pi/2$ pulses and CP is cross polarization, TPPM and CW are different types of decoupling methods that can be applied, while Acq is the acquisition. t_1 and t_2 are the indirect and direct dimensions of the 2D experiment and t_{mix} is the spin diffusion mixing time. (A) Standard DARR experiment, (B) modified DARR experiment with CI setup, (C) two-dimensional ^{13}C–^{13}C photo-CIDNP laser DARR MAS NMR pulse program used for the experiment. Solid bars indicate the $\pi/2$ pulses, Δ is the delay between the laser pulse and the $\pi/2$ pulse on the carbon channel, here $\Delta = 0$ μs, during the ^{13}C mixing time ^{1}H was irradiated under the rotational resonance condition ($\omega_{1H} = n\omega_R$). The phase cycling used in the pulse program is $\Phi_1 = 0\ 2$, $\Phi_2 = 0$, $\Phi_3 = 2$, $\Phi_4 = 0\ 0\ 0\ 0\ 0\ 0\ 0\ 0\ 2\ 2\ 2\ 2\ 2\ 2\ 2\ 2$, $\Phi_5 = 0\ 0\ 0\ 0\ 2\ 2\ 2\ 2$, $\Phi_6 = 0\ 2\ 1\ 3$ and receiver $\Phi_R = 0\ 2\ 1\ 3\ 2\ 0\ 3\ 1\ 2\ 0\ 3\ 1\ 0\ 2\ 1\ 3$. Here definitions are: 0 = +*X*, 1 = +*Y*, 2 = −*X*, 3 = −*Y*.

is used mainly to enhance the ^{13}C polarization, by factor of ~4 by transfer of magnetization from the protons. During the evolution period (t_1) and acquisition, 90 kHz TPPM ^{1}H decoupling was used (total phase difference, 15°, TPPM pulse length 5.5 ms [38]. After the evolution period, the magnetization is tilted along the z-axis with a $\pi/2$ pulse and mixing (t_{mix}) occurs longitudinally with low power irradiation on ^{1}H. The ^{1}H rf field strength is set to the $n = 1$ rotary resonance condition [39].

2.2. Modified DARR for photo-CIDNP under continuous illumination

The modified pulse program using the strong initial ^{13}C polarization provided by the solid-state photo-CIDNP effect is displayed in Fig. 3B. The preparation period has been modified from the standard DARR experiment (Fig. 3A) by replacing the CP segment with a simple ^{13}C $\pi/2$ pulse. Continuous white light is obtained from a 1000 W xenon arc lamp [40].

2.3. Modified DARR for photo-CIDNP under laser-flash illumination

The modified pulse program using the strong initial ^{13}C polarization provided by the solid-state photo-CIDNP effect is displayed in Fig. 3C. The preparation period has been adapted from the standard DARR experiment (Fig. 3A) by removing the CP segment. Advanced photo-CIDNP techniques are used here for selective excitation of the source for the nuclear polarization, and the laser-flash photo-CIDNP segment [41] is incorporated, using a laser light pulse and a subsequent $\pi/2$ pulse. The presaturation of ^{13}C pulses allows for accelerating the experiment by destroying any residual polarization from the previous $\pi/2$ pulse [41].

3. Materials and methods

3.1. Sample preparation

The selective isotopic labelling in RCs of *R. sphaeroides* is achieved by feeding of selectively labelled 3-$^{13}C_1$-δ-aminolevulinic acid (3-ALA), which is a precursor for the formation of BChl and BPhe (Fig. 4), and leads to a ^{13}C enrichment of ~60% [42]. 3-ALA has been purchased from Buchem B.V. (Apeldoorn, The Netherlands).

The RCs were isolated as described earlier [43] and the quinones were removed by incubating the RCs at a concentration of 0.6 μM in 4% LDAO, 10 mM *o*-phenanthroline, 10 mM Tris buffer, pH 8.0, containing 0.025% LDAO and 1 mM EDTA [44]. Approximately 15 mg of RC protein complex embedded in LDAO micelles were used for the NMR experiments.

3.2. MAS NMR experiments

NMR experiments were performed with a DMX-200 NMR spectrometer equipped with a double resonance CP/MAS probe (Bruker-Biospin, Karlsruhe, Germany). The sample was loaded into a clear 4-mm sapphire rotor and inserted into the MAS probe. The sample was frozen at a low spinning frequency of 600 Hz to ensure a homogeneous sample distribution [45]. The light and dark spectra were collected using a Hahn echo pulse sequence with the CYCLOPS phase cycle of the ($\pi/2$) pulse. The data were collected with TPPM carbon–proton decoupling [38] at a temperature of 223 K under continuous illumination with white light [46]. The optimum length of the ($\pi/2$) carbon pulse, determined on uniformly ^{13}C labelled tyrosine, is ~4.0 μs at a strength of 62.5 kHz. The rotational frequency for MAS was 8 kHz. A total number of 128 scans were collected with a recycle delay of 4 s and a line broadening of 10 Hz was applied prior to Fourier transformation. The ^{13}C-MAS NMR spectra were referenced to the $^{13}COOH$ response of solid tyrosine·(HCl) at 172.1 ppm.

3.3. Lamp set up

The continuous illumination setup for the MAS NMR experiments comprises a 1000-W xenon arc lamp with collimation optics, a liquid filter and glass filters, a focusing element and a light fiber. Since the emission spectrum of a Xe lamp is similar to sunlight, the full range of radiation from UV to IR is available for illumination. Disturbance of the spinning frequency counting, which operates from a weak light source in the near-IR region, was avoided by a water filter as well as by various Schott filters such as WG320 and KG3. A fiber bundle was used to transfer the radiation from the collimation optics of the lamp to the sample [2,40].

3.3.1. 2D ^{13}C–^{13}C photo-CIDNP DARR MAS NMR under continuous illumination

All two-dimensional (2D) ^{13}C–^{13}C photo-CIDNP DARR MAS NMR experiments were recorded using a DMX-200 (4.7 T) Bruker console (Bruker-Biospin, Rheinstetten, Germany). The sample has been frozen in the dark. Samples were kept spinning at 8 kHz at a temperature of 223 K under continuous illumination with white light [40]. The DARR pulse program was modified to incorporate the excitation with light (Fig. 3B). For DARR experiments, all spectra were collected with 200t_1 increments and 64 scans, with a recycle delay of 4 s. A spin diffusion mixing time of 1 s was used.

3.4. Laser setup

Using 1064-nm flashes of a Nd:YAG laser (SpectraPhysics Quanta-Ray INDI 40-10, Irvine CA, USA), and frequency-doubling with a second harmonic generator, 532-nm laser flashes were generated with pulse lengths of 6–8 ns and an energy between 20 to 270 mJ. The laser was operating with repetition frequencies between 1 and 4 Hz. Time-resolved photo-CIDNP MAS NMR data were acquired with NMR detection immediately after light excitation, using a presaturation pulse sequence to erase the polarization and coherence from previous scans as described in Daviso et al. [41].

3.4.1. 2D ^{13}C–^{13}C photo-CIDNP laser DARR MAS NMR experiments

The 2D ^{13}C–^{13}C photo-CIDNP laser-flash DARR MAS NMR experiment was recorded with the sample spinning at 8 kHz at a temperature of 223 K using a DMX-200 (4.7 T) Bruker console. The sample was frozen in the dark. The pulse program was modified to incorporate the triggering of the laser pulse CIDNP excitation (Fig. 3C). For laser-flash DARR experiments, all spectra were collected with 100t_1 increments in 3024 scans, with a recycle delay of 4 s. A spin diffusion mixing time of 1 s was used.

3.5. Data processing

All spectra were processed using the TopSpin (version 2.1) software package (Bruker-Biospin, Karlsruhe, Germany). The cosine square (Qsine with SSB = 2) window function was applied along with zero-filling to 1024 data points in both the t_1 and the t_2 dimensions.

3.6. Calculation hyperfine interactions

DFT Calculations of the Radical Cation of the P. DFT computations of hyperfine coupling tensors were performed with the Amsterdam density functional program (ADF) 2002.1 package (SCM NV), using the triple-Zeta basis set with polarization

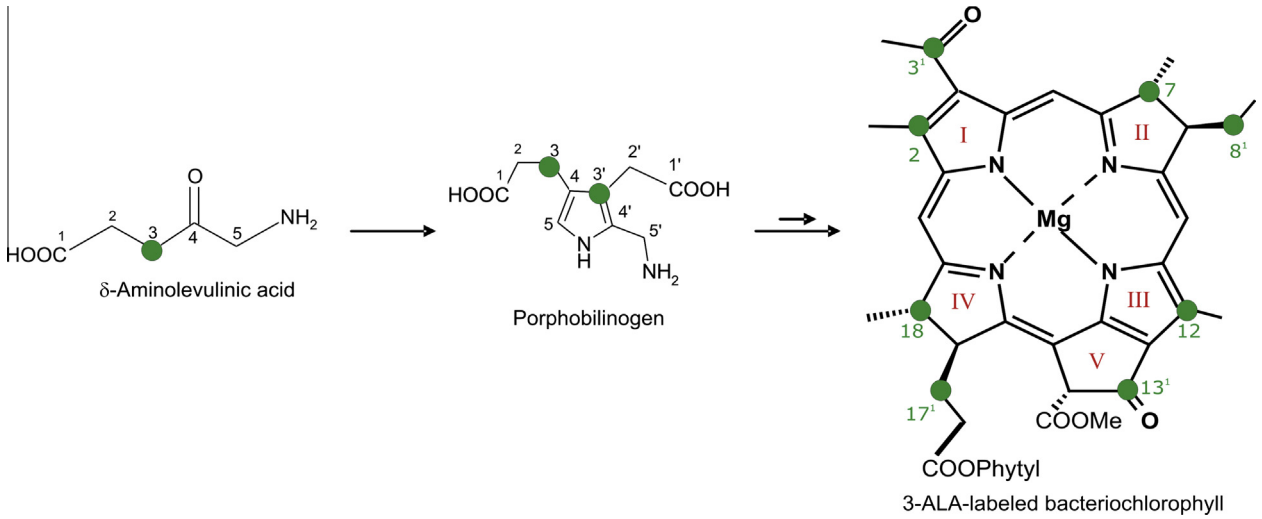

Fig. 4. Biosynthetic pathway for the formation of selectively ^{13}C isotope labelled bacteriochlorophyll *a* (BChl) by feeding the bacteria with 3-$^{13}C_1$-δ-aminolevulinic acid (3-ALA).

functions on all atoms (TZP) all-electron basis set for all atoms as described in Prakash et al. [5] and Daviso et al. [25].

Geometries of ground state molecules were taken from the crystal structure in the charge-neutral state [Protein Data Bank (PDB) ID code 1AIJ] Stowell et al. [47] and subjected to geometry optimization within ADF in the cation radical state.

4. Results and discussion

4.1. 1D ^{13}C MAS NMR experiments

Fig. 5 shows the one-dimensional ^{13}C MAS NMR spectra of 3-ALA labelled RCs of *R. sphaeroides* WT. The data were obtained in a magnetic field of 4.7 T (i.e., 200 MHz ^1H frequency) and at a temperature of 223 K with a MAS frequency of 8 kHz. Fig. 6 provides a detailed view on the carboxylic and aliphatic regions.

Spectrum A in Fig. 5 was collected in the dark, and no signals are observed. Upon CI with white light, strong polarization is established (Spectrum B in Figs. 5 and 6). All signals are light-induced and emissive (negative). The sign of the signal has been explained by the dominance of the TSM over the DD mechanism [4]. The two strongest signals at 119.4 and 134.2 ppm have been assigned to the C-12 and C-2 carbons, respectively. The strong solid-state photo-CIDNP effect confirms that these aromatic carbons obtain direct strong enhancement from the electron spin that is delocalized over aromatic system of the special pair [2]. All other signals are considerably weaker. At least four signals can be clearly distinguished in the carbonyl region. The carbonyl carbon atoms are labelled and may gain intensity from the nearby C-2 and C-12 that are strongly polarized. The intensity of the signals in the aliphatic region between 0 and 60 ppm is less than for the signals in the aromatic region. Since for unlabelled RCs under continuous illumination, virtually no photo-CIDNP arises at aliphatic carbons [4], the observed

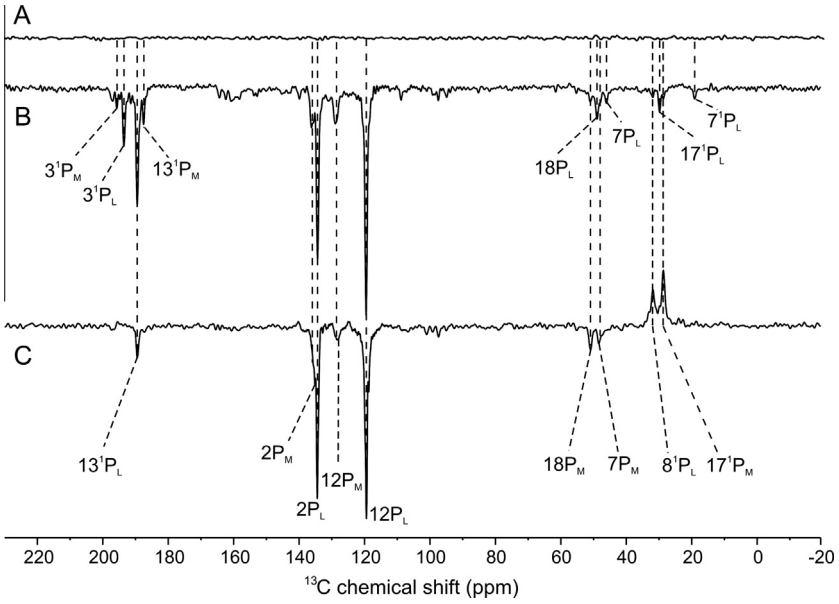

Fig. 5. One-dimensional ^{13}C photo-CIDNP MAS NMR spectra of 3-ALA labelled RCs of *R. sphaeroides* WT (A) in the dark, (B) under continuous light and (C) under nanosecond laser-flash with delay $\Delta = 0$ ms.

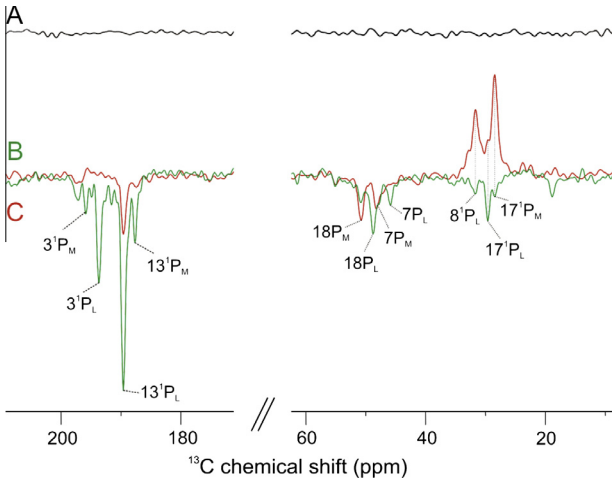

Fig. 6. Carbonyl and aliphatic regions of one-dimensional ^{13}C photo-CIDNP MAS NMR spectra of 3-ALA labelled RCs of *R. sphaeroides* WT (A) in the dark, (B) under continuous light and (C) under nanosecond laser-flash with delay Δ = 0 ms.

intensity gain in the 1D experiments is attributed to transfer from strongly polarized aromatic carbons by ^{13}C spin diffusion to the aliphatic periphery.

In Spectrum C in Figs. 5 and 6, photo-CIDNP is induced by laser flashes, immediately followed by NMR detection. Compared to the continuous illumination experiment, the signals are both absorptive and emissive since the phase signs of the signals in this spectrum are determined by Kaptein's rule [26]. The occurrence of both emissive and enhanced absorptive lines makes signal assignment easier by referring to calculated local electron spin densities (Tables 2a–2c).

5. 2D ^{13}C–^{13}C photo-CIDNP DARR MAS NMR spectra

In Fig. 7, the 2D ^{13}C–^{13}C photo-CIDNP DARR MAS NMR spectra of 3-ALA labelled RCs of *R. sphaeroides* WT are shown which have been obtained under CI with white light (A) and under flash-laser excitation (B). In both cases, the spin-diffusion mixing time was 1 s. In addition to the diagonal peaks, several cross peaks are observed. Many carbons of the BChl cofactors of the special pair have been already assigned in previous studies on unlabelled [4,5], 4-ALA [25,42] and 5-ALA [48] labelled WT RCs. While the 4- and 5-ALA label patterns allow to study the aromatic carbons of the BChl and BPhe macrocycles, 3-ALA labelling leads to isotope enrichment of the more peripheral carbon positions (Figs. 1 and 4). This label pattern is particularly suitable for observation of spin diffusion since it allows for sufficient chemical-shift dispersion for convenient separation of signals.

Table 2a
IUPAC numbers of the P_M and their respective calculated values of a_{iso} and ΔA.

Carbon's position in P_M	a_{iso} (MHz)	ΔA (MHz)
1	1.7731	9.5919
2	1.6897	9.3966
3	−1.9722	0.2773
4	3.605	11.0715
5	−3.4790	1.7564
6	4.8412	13.4397
7	−1.3268	0.5416
8	−1.6062	0.3848
9	4.8848	14.6508
10	−2.8147	0.5566
11	1.6644	10.5769
12	2.1074	12.0685
13	−2.0735	0.614
14	3.5553	10.843
15	−3.8828	1.9422
16	5.8395	15.6412
17	−1.6268	0.3458
18	−1.4505	0.2939
19	4.78	13.977
20	−3.0592	1.2769
2^1	−1.1780	0.4416
3^1	−0.0643	0.1084
3^2	−0.0091	0.1505
7^1	5.433	0.9927
8^1	5.426	1.1174
8^2	0.1023	0.279
12^1	−1.5083	0.3457
13^1	−0.4788	0.3528
13^2	0.0875	0.1821
13^3	−0.8577	0.2021
13^4	0.0472	0.1121
17^1	4.5759	1.1575
17^2	−0.0690	0.3259
17^3	0.0443	0.0973
18^1	5.2977	0.9557

5.1. Continuous illumination 2D ^{13}C–^{13}C photo-CIDNP DARR MAS NMR spectrum

In photo-CIDNP MAS NMR spectra on RCs of *R. sphaeroides* WT, signals from three cofactors are enhanced, the two BChl cofactors of the special pair and the primary electron acceptor BPhe in the active A branch [42]. In the DARR spectrum A of Fig. 7, obtained under CI, however, two networks are observed only, which can be conveniently assigned to the two BChl cofactors of the special pair. The more extended network is labelled in blue and is assigned to cofactor P_L of the special pair carrying higher electron spin density [4,49]. It represents a complete set of correlation signals for eight carbon nuclei, including the responses from the C-2 and the C-12 with the strongest intensities. From this network, a complete set of eight chemical shift assignments have been obtained (Table 1) matching to known resonances of P_L. A second network, labelled in red, is from a spin system comprising five ^{13}C nuclei,

Table 1
Assignment of the signals from 3-ALA-labelled bacterial RCs obtained with continuous illumination and nanosecond laser-flash excitation, with their respective signs of polarization. For the continuous illumination experiment all the polarization is emissive. (E = emissive; A = absorptive).

Carbon's position in BChl *a*	P_L	Sign in laser expt	P_M	Sign in laser expt	BPhe
2	134.3	E	136.2	E	
3^1	193.5	–	195.6	–	
7	46.1	–	48.3	E	
8^1	32.1	A			
12	119.5	E	128.8	E	126.9
13^1	189.4	E	187.5	–	
17^1	29.9	A	28.4	A	
18	49.1	–	50.9	E	
7^1	19.1	–		–	

Table 2b
IUPAC numbers of the P_L and their respective calculated values of a_{iso} and ΔA.

Carbon's position in P_L	a_{iso} (MHz)	ΔA (MHz)
1	2.8829	14.3282
2	2.158	13.113
3	−2.3671	1.7295
4	5.2484	15.8799
5	−4.7583	2.269
6	7.0186	19.1645
7	−1.9269	0.6833
8	−2.2206	0.3978
9	6.8934	20.1713
10	−4.5494	1.6325
11	2.6737	15.545
12	2.806	16.5525
13	−2.6225	1.3671
14	4.7728	14.7333
15	−5.3101	2.2941
16	9.2318	24.4369
17	−2.5917	0.5872
18	−2.0785	0.6113
19	8.0712	20.8362
20	−4.4822	1.9127
2^1	−1.6535	0.307
3^1	−0.5444	0.3567
3^2	−0.1322	0.1365
7^1	6.8887	1.3155
8^1	7.4891	1.5265
8^2	0.1731	0.4405
12^1	−2.0383	0.5073
13^1	−0.7157	0.4978
13^2	0.2166	0.2119
13^3	−1.2329	0.1742
13^4	−0.0330	0.0622
17^1	8.7024	1.7612
17^2	0.0819	0.417
17^3	−0.0411	0.115
18^1	8.8269	1.5838

Table 2c
IUPAC numbers of the Φ_A and their respective calculated values of a_{iso} and ΔA.

Carbon's position in Φ_A	a_{iso} (MHz)	ΔA (MHz)
1	−4.0898	7.5168
2	8.4399	33.5792
3	−0.5842	12.9589
4	−3.6908	0.8122
5	6.2948	22.1958
6	−6.4808	2.868
7	0.1378	0.3274
8	0.1277	0.2887
9	−5.8094	1.9962
10	5.1275	19.8083
11	−3.7464	5.2241
12	7.4997	28.5875
13	−1.9219	8.8494
14	−4.0378	0.9188
15	8.0234	25.5863
16	−7.9137	3.6307
17	0.2288	0.3256
18	−0.2166	0.348
19	6.2948	22.1958
20	6.1744	24.4854
2^1	−4.3718	0.6735
3^1	1.4387	10.9881
3^2	−1.8654	0.2722
7^1	−0.3147	0.3033
8^1	−0.5471	0.2329
8^2	0.3963	0.2511
12^1	−3.6127	0.4828
13^1	1.5118	10.8316
13^2	−4.0240	0.203
13^3	0.4748	0.4701
13^4	−0.0560	0.1806
17^1	−0.6292	0.2518
17^2	0.1759	0.1519
17^3	−0.0083	0.0801
18^1	0.8611	0.3309

and is assigned to cofactor P_M. As observed previously, most of the signals assigned to P_L are shielded compared to the signals of P_M [4,27,42,48]. In particular the difference between the chemical shifts of the C-12 atoms of 9.0 ppm is remarkable and demonstrates the significant ground-state asymmetry within the dimer [42]. Hence, 2D CI experiments allow for full analysis of the electronic ground state

5.2. Time-resolved 2D ^{13}C–^{13}C photo-CIDNP DARR MAS NMR spectrum

Fig. 7B shows the two-dimensional ^{13}C–^{13}C photo-CIDNP laser-flash DARR MAS NMR spectra of 3-ALA labelled RCs of *R. sphaeroides* WT collected at 223 K with a delay time (Δ) between the laser excitation pulse and NMR detection pulse of 0 μs and a spin-diffusion mixing time of 1 s at a MAS frequency of 8 kHz. In time-resolved experiments on RCs of *R. sphaeroides* WT with virtually no delay time Δ, the light-induced signals are mainly due to the transient nuclear polarization as explained above (Fig. 2) [25]. Hence, the laser-flash ^{13}C–^{13}C correlation experiment provides both a view on the electronic structure as well as chemical shift assignments of the labelled atoms in the special pair.

In the time-resolved two-dimensional spectrum, mainly peaks from P_L appear and only a few from P_M (Table 1). In the one-dimensional dataset collected with laser-flash excitation, the signals in the aliphatic region are relatively strong compared to the CI experiment (Fig. 6, right part) and the signals from C-17^1P_M, C-17^1P_L and C-8^1P_L are absorptive. In Fig. 7, selected regions of 2D spectra are displayed. Since Fig. 7A is obtained with CI, all diagonal peaks are emissive, which leads to completely emissive sets of cross peaks. The cross peak intensities confirm that the signal strength is transferred along the f_2 dimension. For example, the cross peak, C-12P_L/C-7^1P_L is very pronounced, as the corresponding diagonal peak in the f_2 direction is also strong. In Fig. 7B, laser flashes were used as source of the photo-CIDNP enhancement and both absorptive and emissive signals occur. The cross peaks in the aliphatic region, for example, C-18P_M/C-17^1P_M show the same sign as the diagonal peaks along the f_2 dimension (see dashed arrows).

Compared to the continuous illumination experiment, in time-resolved experiments, though the signs of the peak directly follow the Kaptein's rules. It should be noted that different orientations contribute differently to the RPM because of the anisotropy of the g factor difference. Hence, if hyperfine anisotropy is much larger than the isotropic hyperfine coupling, the orientation average of RPM is not necessarily proportional to a_{iso}. For the nuclei where the isotropic hyperfine coupling dominates the anisotropic coupling (C-17^1P_M, C-8^1P_L, C-7P_M, C-18P_M, C-3^1P_L), so that the sign of the hyperfine coupling is the same at all orientations, the sign of the signal agrees with the sign of a_{iso}. For strong hyperfine anisotropy (C-2P_L, C-12P_L, C-2P_M, C-12P_M) negative signals are observed even if a_{iso} is positive, which may result from contributions by the TSM/DD solid-state CIDNP mechanisms or from weighted orientation averaging of the RPM contributions. For dominating hyperfine anisotropy, orientations with negative as well as positive sign of the hyperfine coupling exist and the signal contribution also depends on the anisotropic *g* value difference between donor and acceptor [25,27]. Therefore fewer diagonal peaks are observed for the same mixing time of 1s. Hence, the enhancement mechanism in the 2D laser-DARR acts as a filter for correlation experiments. The higher selectivity also allows for clarifying the assignments for C-7P_M, C-7P_M, C-8P_L and C-18P_M. (Table 1).

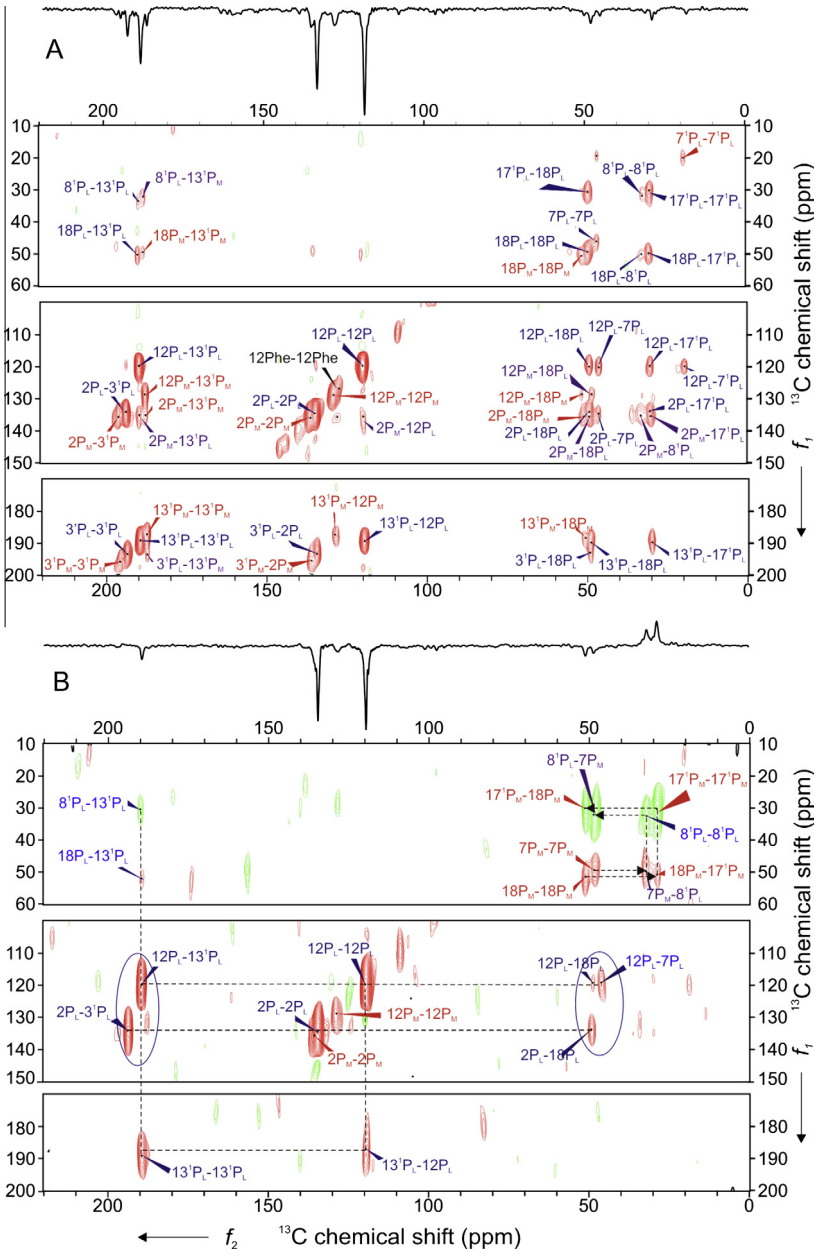

Fig. 7. Two-dimensional ^{13}C–^{13}C photo-CIDNP DARR MAS NMR spectra of 3-ALA labelled RCs of *R. sphaeroides* WT with a spin-diffusion mixing time of 1 s, collected with a spinning frequency of 8 kHz at a temperature of 223 K. (A) Light source used is a 1000-W xenon lamp. (B) Data obtained with the nanosecond-flash laser setup. Circled region displayed less number of cross peaks in laser experiment compared to the same regions with CI experiment. Red peaks represent absorptive signals while green peaks represent emissive signals. (For interpretation of the references to color in this figure legend, the reader is referred to the web version of this article.)

6. Conclusions

The complex signal pattern observed in the photo-CIDNP MAS 2D NMR experiment spectrum under CI has been filtered and edited in the time-resolved experiment by the values and signs of isotropic (a_{iso}) and anisotropic (ΔA) hyperfine interaction. This method allows to refine assignments and to validate calculated local electron spin densities. In addition, local electron spin densities can be directly mapped from radical pairs, due to the strong photo-CIDNP enhancement, even when they originate from membrane bound proteins.

References

[1] G. Jeschke, J. Matysik, A reassessment of the origin of photochemically induced dynamic nuclear polarization effects in solids, Chem. Phys. 294 (2003) 239–255.
[2] E. Daviso, G. Jeschke, J. Matysik, Photochemically induced dynamic nuclear polarization (Photo-CIDNP) magic-angle spinning NMR, in: T. Aartsma, J. Matysik (Eds.), Biophysical Techniques in Photosynthesis II, Springer, Dordrecht, 2008, pp. 385–399.
[3] M.G. Zysmilich, A. McDermott, Photochemically induced dynamic nuclear-polarization in the solid-state ^{15}N spectra of reaction centers from photosynthetic bacteria *Rhodobacter sphaeroides* R-26, J. Am. Chem. Soc. 116 (1994) 8362–8363.
[4] S. Prakash, Alia, P. Gast, H.J.M. de Groot, G. Jeschke, J. Matysik, Magnetic field dependence of photo-CIDNP MAS NMR on photosynthetic reaction centers of *Rhodobacter sphaeroides* WT, J. Am. Chem. Soc. 127 (2005) 14290–14298.
[5] S. Prakash, Alia, P. Gast, H.J.M. de Groot, J. Matysik, G. Jeschke, Photo-CIDNP MAS NMR in intact cells of *Rhodobacter sphaeroides* R-26: Molecular and atomic resolution at nanomolar concentration, J. Am. Chem. Soc. 128 (2006) 12794–12799.
[6] E. Roy, T. Rohmer, P. Gast, G. Jeschke, A. Alia, J. Matysik, Characterization of the primary radical pair in reaction centers of *Heliobacillus mobilis* by ^{13}C Photo-CIDNP MAS NMR, Biochemistry 47 (2008) 4629–4635.
[7] S.S. Thamarath, B.E. Bode, S. Prakash, K.B. Sai Sankar Gupta, A. Alia, G. Jeschke, J. Matysik, Electron spin density Distribution in the special pair Triplet of *Rhodobacter sphaeroides* R26 revealed by magnetic field dependence of the solid-state Photo-CIDNP effect, J. Am. Chem. Soc. 134 (2012) 5921–5930.

[8] A. Diller, A. Alia, P. Gast, G. Jeschke, J. Matysik, ^{13}C Photo-CIDNP MAS NMR on the LH1-RC complex of *Rhodopseudomonas acidophila*, in: Photosynthesis. Energy from the Sun, 2008, pp. 55–58.
[9] E. Roy, Alia, P. Gast, H. van Gorkom, H.J.M. de Groot, G. Jeschke, J. Matysik, Photochemically induced dynamic nuclear polarization in the reaction center of the green sulphur bacterium *Chlorobium tepidum* observed by ^{13}C MAS NMR, Biochim. Biophys. Acta – Bioenerg. 1767 (2007) 610–615.
[10] J. Matysik, Alia, P. Gast, H.J. van Gorkom, A.J. Hoff, H.J.M. de Groot, Photochemically induced nuclear spin polarization in reaction centers of photosystem II observed by ^{13}C-solid-state NMR reveals a strongly asymmetric electronic structure of the P680.+ primary donor chlorophyll, Proc. Natl. Acad. Sci. U. S. A 97 (2000) 9865–9870.
[11] A. Alia, E. Roy, P. Gast, H.J. van Gorkom, H.J.M. de Groot, G. Jeschke, J. Matysik, Photochemically induced dynamic nuclear polarization in photosystem I of plants observed by ^{13}C magic-angle spinning NMR, J. Am. Chem. Soc. 126 (2004) 12819–12826.
[12] A. Diller, E. Roy, P. Gast, H.J. van Gorkom, H.J.M. de Groot, C. Glaubitz, G. Jeschke, J. Matysik, A. Alia, ^{15}N photochemically induced dynamic nuclear polarization magic-angle spinning NMR analysis of the electron donor of photosystem II, Proc. Natl. Acad. Sci. U. S. A. 104 (2007) 12767–12771.
[13] G.J. Janssen, E. Daviso, M. van Son, H.J.M. de Groot, A. Alia, J. Matysik, Observation of the solid-state photo-CIDNP effect in entire cells of cyanobacteria Synechocystis, Photosynth. Res. 104 (2010) 275–282.
[14] J. Matysik, A. Diller, E. Roy, A. Alia, The solid-state photo-CIDNP effect, Photosynth. Res. 102 (2009) 427–435.
[15] S. Thamarath Surendran, J. Heberle, P.J. Hore, T. Kottke, J. Matysik, Solid-state photo-CIDNP effect observed in phototropin LOV1-C57S by ^{13}C magic-angle spinning NMR spectroscopy, J. Am. Chem. Soc. 132 (2010) 15542–15543.
[16] A.J. Hoff, J. Deisenhofer, Photophysics of photosynthesis. Structure and spectroscopy of reaction centers of purple bacteria, Phys. Rep. – Rev. Sect. Phys. Lett. 287 (1997) 2–247.
[17] R.E. Blankenship, G.T. Babcock, J.T. Warden, K. Sauer, Observation of a new EPR transient in chloroplasts that may reflect electron-donor to photosystem II at room-temperature, FEBS Lett. 51 (1975) 287–293.
[18] A.J. Hoff, H. Rademaker, R. Vangrondelle, L.N.M. Duysens, Magnetic-field dependence of yield of triplet-state in reaction centers of photosynthetic bacteria, Biochim. Biophys. Acta 460 (1977) 547–554.
[19] G.L. Closs, L.E. Closs, Induced dynamic nuclear spin polarization in reactions of photochemically and thermally generated triplet diphenylmethylene, J. Am. Chem. Soc. 91 (1969) 4549.
[20] R. Kaptein, J.L. Oosterhoff, Chemically induced dynamic nuclear polarization II: (Relation with anomalous ESR spectra), Chem. Phys. Lett. 4 (1969) 195.
[21] G. Jeschke, Electron–electron–nuclear three-spin mixing in spin-correlated radical pairs, J. Chem. Phys. 106 (1997) 10072–10086.
[22] G. Jeschke, A new mechanism for chemically induced dynamic nuclear polarization in the solid state, J. Am. Chem. Soc. 120 (1998) 4425–4429.
[23] T. Polenova, A.E. McDermott, A coherent mixing mechanism explains the photoinduced nuclear polarization in photosynthetic reaction centers, J. Phys. Chem. B 103 (1999) 535–548.
[24] A. Diller, S. Prakash, A. Alia, P. Gast, J. Matysik, G. Jeschke, Signals in solid-state photochemically induced dynamic nuclear polarization recover faster than signals obtained with the longitudinal relaxation time, J. Phys. Chem. B 111 (2007) 10606–10614.
[25] E. Daviso, A. Alia, S. Prakash, A. Diller, P. Gast, J. Lugtenburg, J. Matysik, G. Jeschke, Electron–nuclear spin dynamics in a bacterial photosynthetic reaction center, J. Phys. Chem. C 113 (2009) 10269–10278.
[26] R. Kaptein, Simple rules for chemically induced dynamic nuclear polarization, Chem. Commun. 14 (1971) 732–733.
[27] E. Daviso, S. Prakash, A. Alia, P. Gast, J. Neugebauer, G. Jeschke, J. Matysik, The electronic structure of the primary electron donor of reaction centers of purple bacteria at atomic resolution as observed by photo-CIDNP ^{13}C NMR, Proc. Natl. Acad. Sci. U. S. A. 106 (2009) 22281–22286.
[28] R. Tycko, G. Dabbagh, Measurement of nuclear magnetic dipole–dipole couplings in magic angle spinning NMR, Chem. Phys. Lett. 173 (1990) 461–465.
[29] A.E. Bennett, R.G. Griffin, J.H. Ok, S. Vega, Chemical shift correlation spectroscopy in rotating solids: radio frequency-driven dipolar recoupling and longitudinal exchange, J. Chem. Phys. 96 (1992) 8624–8627.
[30] A.E. Bennett, C.M. Rienstra, J.M. Griffiths, W. Zhen, J.P.T. Lansbury, R.G. Griffin, Homonuclear radio frequency-driven recoupling in rotating solids, J. Chem. Phys. 108 (1998) 9463–9479.
[31] Y.K. Lee, N.D. Kurur, M. Helmle, O.G. Johannessen, N.C. Nielsen, M.H. Levitt, Efficient dipolar recoupling in the NMR of rotating solids – a sevenfold symmetrical radiofrequency pulse sequence, Chem. Phys. Lett. 242 (1995) 304–309.
[32] N.M. Szeverenyi, M.J. Sullivan, G.E. Maciel, Observation of spin exchange by two-dimensional Fourier-transform C13 cross polarization-magic-angle spinning, J. Magn. Reson. 47 (1982) 462–475.
[33] A. Grommek, B.H. Meier, M. Ernst, Distance information from proton-driven spin diffusion under MAS, Chem. Phys. Lett. 427 (2006) 404–409.
[34] K. Takegoshi, S. Nakamura, T. Terao, ^{13}C–^{1}H dipolar-assisted rotational resonance in magic angle spinning NMR, Chem. Phys. Lett. 344 (2001) 631–637.
[35] N. Nielsen, L. Strassø, A. Nielsen, Dipolar recoupling, in: J.C.C. Chan (Ed.), Solid State NMR, Springer, Berlin Heidelberg, 2012, pp. 1–45.
[36] S. Dusold, A. Sebald, Dipolar recoupling under magic-angle spinning conditions, in: Annual Reports on NMR Spectroscopy, Academic Press, 2000, pp. 185–264.
[37] M. Veshtort, R.G. Griffin, Proton-driven spin diffusion in rotating solids via reversible and irreversible quantum dynamics, J. Chem. Phys. 135 (2011) 134509.
[38] A.E. Bennett, C.M. Rienstra, M. Auger, K.V. Lakshmi, R.G. Griffin, Heteronuclear decoupling in rotating solids, J. Chem. Phys. 103 (1995) 6951–6958.
[39] N.C. Nielsen, F. Creuzet, R.G. Griffin, M.H. Levitt, Enhanced double-quantum nuclear magnetic resonance in spinning solids at rotational resonance, J. Chem. Phys. 96 (1992) 5668.
[40] J. Matysik, Alia, J. Holland, T. Egorova-Zachernyuk, P. Gast, H.J.M. de Groot, Sample illumination and photo-CIDNP in a magic-angle spinning NMR probe, Indian J. Biochem. Biophys. 37 (2000) 418–423.
[41] E. Daviso, A. Diller, A. Alia, J. Matysik, G. Jeschke, Photo-CIDNP MAS NMR beyond the T_1 limit by fast cycles of polarization extinction and polarization generation, J. Magn. Reson. 190 (2008) 43–51.
[42] E.A.M. Schulten, J. Matysik, Alia, S. Kiihne, J. Raap, J. Lugtenburg, P. Gast, A.J. Hoff, H.J.M. de Groot, ^{13}C MAS NMR and photo-CIDNP reveal a pronounced asymmetry in the electronic ground state of the special pair of *Rhodobacter sphaeroides* reaction centers, Biochemistry 41 (2002) 8708–8717.
[43] S. Shochat, T. Arlt, C. Francke, P. Gast, P.I. Vannoort, S.C.M. Otte, H.P.M. Schelvis, S. Schmidt, E. Vijgenboom, J. Vrieze, W. Zinth, A.J. Hoff, Spectroscopic characterization of reaction centers of the (M)Y210W mutant of the photosynthetic bacterium *Rhodobacter sphaeroides*, Photosynth. Res. 40 (1994) 55–66.
[44] M.Y. Okamura, R.A. Isaacson, G. Feher, Primary acceptor in bacterial photosynthesis – obligatory role of ubiquinone in photoactive reaction centers of *Rhodopseudomonas spheroides*, Proc. Natl. Acad. Sci. U. S. A. 72 (1975) 3491–3495.
[45] M.R. Fischer, H.J.M. Degroot, J. Raap, C. Winkel, A.J. Hoff, J. Lugtenburg, ^{13}C magic angle spinning NMR-study of the light-induced and temperature-dependent changes in *Rhodobacter sphaeroides* R-26 reaction centers enriched in 4′-^{13}C tyrosine, Biochemistry 31 (1992) 11038–11049.
[46] J. Matysik, E. Schulten, Alia, P. Gast, J. Raap, J. Lugtenburg, A.J. Hoff, H.J.M. de Groot, Photo-CIDNP 13C magic angle spinning NMR on bacterial reaction centres: exploring the electronic structure of the special pair and its surroundings, Biol. Chem. 382 (2001) 1271–1276.
[47] M.H.B. Stowell, T.M. McPhillips, D.C. Rees, S.M. Soltis, E. Abresch, G. Feher, Light-induced structural changes in photosynthetic reaction center: implications for mechanism of electron–proton transfer, Science 276 (1997) 812–816.
[48] S. Prakash, A. Alia, P. Gast, H.J.M. de Groot, G. Jeschke, J. Matysik, ^{13}C chemical shift map of the active cofactors in photosynthetic reaction centers of *Rhodobacter sphaeroides* revealed by photo-CIDNP MAS NMR, Biochemistry 46 (2007) 8953–8960.
[49] A. Marchanka, W. Lubitz, M. van Gastel, Spin density distribution of the excited triplet state of bacteriochlorophylls. Pulsed ENDOR and DFT studies, J. Phys. Chem. B 113 (2009) 6917–6927.